Brain Structure and Function (2019) 224:1947–1956
https://doi.org/10.1007/s00429-019-01861-5

METHODS PAPER

PICS: a platform for planar imaging of curved surfaces of brain and other tissue

Jessica L. Scoggin[1] · Benjamin S. Kemp[1] · Daniel A. Rivera[1,2] · Teresa A. Murray[1]

Received: 31 August 2018 / Accepted: 12 March 2019 / Published online: 22 March 2019

Abstract

Optical imaging of wholemount tissue samples provides greater understanding of structure–function relationships as the architecture of these specimens is generally well preserved. However, difficulties arise when attempting to stitch together images of multiple regions of larger, oddly shaped specimens. These difficulties include (1) maintaining consistent signal-to-noise ratios when the overlying sample surface is uneven, (2) ensuring sample viability when live samples are required, and (3) stabilizing the specimen in a fixed position in a flowing medium without distorting the tissue sample. To address these problems, we designed a simple and cost-efficient device that can be 3D-printed and machined. The design for the device, named the Platform for Planar Imaging of Curved Surfaces (PICS), consists of a sample holder, or "cap" with gaps for fluid flow and a depression for securing the sample in a fixed position without glue or pins, a basket with two arms that move along an external radius to rotate the sample around a central axis, and a customizable platform designed to fit on a commercially available temperature control system for slice electrophysiology. We tested the system using wholemounts of the murine subventricular zone (SVZ), which has a high degree of curvature, to assess sample viability and image quality through cell movement for over an hour for each sample. Using the PICS system, tissues remained viable throughout the imaging sessions, there were no noticeable decreases in the image SNR across an imaging plane, and there was no noticeable displacement of the specimen due to fluid flow.

Keywords Wholemount imaging · Multiphoton imaging · 3D printing · Open source design · Subventricular zone · Cytoarchitecture

Introduction

Imaging of intact tissue samples, also referred to as wholemounts (Darnell et al. 2010; Graydon and Giorgi 1984; Mirzadeh et al. 2010a; Nagasawa and Yanai 1977), in small animals is important for understanding unique structure–function relationships not otherwise observed in fixed and sectioned samples of tumors, glands, and parts of the brain, such as the subventricular zone (SVZ). Several sets of high-resolution images from adjacent areas can be stitched together in a planar mosaic image that enables visualization across a layer of interest within the tissue while capturing cellular and subcellular features (Thévenaz and Unser 2007).

Trade-offs exist between using fixed and live wholemounts. When using fixed or fixed and cleared (Parra et al. 2010) wholemounts for imaging, the benefit of having long periods of time to acquire 2D images for mosaics or 3D images (z-stacks) is offset by the inability to acquire dynamic, functional information. On the other hand, using live wholemount tissue permits acquisition of dynamic, functional data, such as migrating cells or calcium dynamics. In the SVZ, for example, the use of live wholemounts has been used to assess neuroblast migration rates and trajectories and for cerebrospinal fluid flow studies (Comte et al. 2011; Mirzadeh et al. 2010b; Platel et al. 2008).

Image scans can be acquired quickly enough to avoid issues with degradation in live wholemounts that have

Electronic supplementary material The online version of this article (https://doi.org/10.1007/s00429-019-01861-5) contains supplementary material, which is available to authorized users.

✉ Teresa A. Murray
tmurray@latech.edu; bioengineer1@hotmail.com

[1] Center for Biomedical Engineering and Rehabilitation Sciences, Louisiana Tech University, PO Box 10157, Ruston, LA 71272-0046, USA

[2] Nancy E. and Peter C. Meinig School of Biomedical Engineering, Cornell University, Ithaca, NY, USA

surfaces or layers in a relatively planar orientation parallel to the microscope stage. Yet, numerous structures of interest have curved surfaces or profiles, such as the lumens of intestines (Hagl et al. 2013) and bronchial tubes (Rosewell and Giangreco 2012), retinas (Ullmann et al. 2012), tumor boundaries (Cyran et al. 2014), embryos (Udan et al. 2014), heart ventricles (Zhou and Pu 2011), and interfaces between brain regions (Sasaki and Hogan 1993). In the brain, curved regions of structural and functional interest include the lateral ventricles, which possess ciliated epithelium and a dynamic neurogenic niche (Young et al. 2013; Goings et al. 2004).

An important consideration in optical imaging is that light transmission decays exponentially as a function of tissue depth due to absorbance and scattering of light through tissue (Cheong et al. 1990). The thickness of overlying tissue often varies when sections are cut in blocks, resulting in non-uniform signal-to-noise ratio across the field of view of a curved layer, with deeper parts having the poorest optical signal. This can be mitigated by cutting a curved section with a more uniform depth of overlying tissue, or by opening the structure, such as SVZ wholemount preparations, so that the curved layer of interest is exposed. However, this can create irregularly shaped tissue samples with a curved surface.

To capture images of dynamic events in living tissue with curved regions of interest, such as stem cell migration along the lateral ventricles of the rodent brain, the operator must constantly adjust the height of the microscope objective (or microscope stage) while also adjusting the *x*–*y* position of the stage to acquire images that can be joined into image mosaics. This is time-consuming and imposes a severe limitation on the amount of live tissue that can be imaged before the tissue degrades. Alternatively, the operator can change the angle of orientation of the sample, enabling imaging of more of a planar-like surface and providing a more uniform signal-to-noise ratio of the acquired images. Unfortunately, it is easy to lose the site of interest when repositioning tissue. In addition, the researcher may be forced to unpin or scrape glued tissue, if adhered, to capture the curved structure. Both unpinning then repinning or scraping then readhering may cause significant damage to the tissue, and reduce the number of images acquired before the tissue degrades. Furthermore, warmed, oxygenated media must constantly flow around live tissue to maintain viability. Fluid flow can cause tissue to shift over time. Pinning tissue to prevent movement, however, can distort the natural shape of the tissue.

To overcome these imaging issues, a device for planar imaging of curved surfaces (PICS) was created. PICS does not use adhesive or pins to hold the sample in place during sample rotation and when media flows around live samples. Furthermore, the device fits onto a commercially available, low profile system for ex vivo imaging that controls the temperature, and flow rate of warmed media for maintaining live tissue. The basket and sample cap designs can be modified to image smaller or larger tissue samples and tissue with a different radius of curvature. Design files for producing the devices are freely available to enable researchers to produce and modify PICS for different imaging applications. The following sections describe how this device was designed, tested, and used for an ex vivo study of the SVZ using wholemounts from murine brains.

The SVZ is one of two main regions in the brain where neurogenesis occurs in mice as well as humans (Lennington et al. 2003; Strien et al. 2011; Wang et al. 2011). In the SVZ, quiescent neural stem cells (type B cells) give rise to transit-amplifying cells (type C cells) which form neuroblasts (type A cells). In rodents, neuroblasts formed in this region travel in chains down the rostral migratory stream to the olfactory bulb where they become interneurons (Martinez-Molina et al. 2011). There is a large interest in studying the native structure and function of this neurogenic niche, as well as its roles in development and brain injury, due to the therapeutic potential of neuronal progenitors (Chang et al. 2016; Shen et al. 2008; Strien et al. 2011; Young et al. 2011).

Wholemount tissue samples are often used to visualize the SVZ. This technique involves micro-dissecting an extracted brain tissue sample to expose the walls of the lateral ventricle (Mirzadeh et al. 2010a). Wholemounts better preserve the cytoarchitecture of the SVZ than other histological techniques (Mirzadeh et al. 2010a), allowing researchers to analyze the natural pathways, normal relationships, and typical mechanisms of resident stem cells. Dynamic processes such as motility and dispersion can also be studied through time-lapse imaging of living lateral ventricular wall wholemounts (LVWMs).

The lateral ventricles of the SVZ retain their curved structure following dissection (Fiorelli et al. 2015), making them difficult to image using a traditional microscope system. Most microscopes are fitted with a flat stage, resulting in a planar range of motion. When the curved surface of the LVWM is placed under the microscope objective lens, structures that form an uninterrupted surface must be viewed in different planes of focus by vertically repositioning either the stage, the microscope objective lens, or by adjusting the tissue in relation to the objective lens. Refocusing on the sample after each movement of the stage or adjusting the tissue is also time-consuming and causes the researcher to painstakingly piece together a single, continuous image of the surface out of multiple stacks of data.

Materials and methods

PICS platform design and construction

The PICS platform was designed to stabilize the LVWM while facilitating rotation of the curved surface with respect to a microscope objective for more efficient image

capture. In addition, the PICS platform was designed to allow fluid flow around the tissue, keeping cells viable, to prevent shear stress on the tissue, to ensure rotation of the sample without unwanted translation, and to securely attach to a commercially available environmental controller.

To meet our objective, the PICS system was designed, such that the tissue sample would be rotated around the microscope objective lens in a manner that would keep the curved region of interest in focus as the sample is slowly rotated. PICS components were then designed individually in SolidWorks® (Dassault Systèmes), with design iterations focused on movement of the tissue sample with a desired radius of curvature and sample stability. The final PICS design consists of a 3D printed bottom plate (Fig. 1a) with clips (Fig. 1b), a sample cap (Fig. 1c), and a machine milled basket (Fig. 1d). The tissue sample fits into the cap (C) which is then placed into the basket (D). This complete configuration (Fig. 1e) allows for both radial rotation of the cap and axial rotation of the basket along the baseplate archway (see Fig. 5 for radial and axial rotation examples with actual device).

The system consists of both three-dimensionally (3D) printed and machine milled parts. A MakerBot® Replicator® 2 3D printer and polylactic acid (PLA) filament were used to fabricate the printed parts, which are the baseplate and clips. The machined components were composed of polycarbonate (PC). PC machined parts include the basket and sample cap (SolidWorks® design files are available at https://3dprint.nih.gov/discover/3dpx-009586; instructions are in Appendix 1).

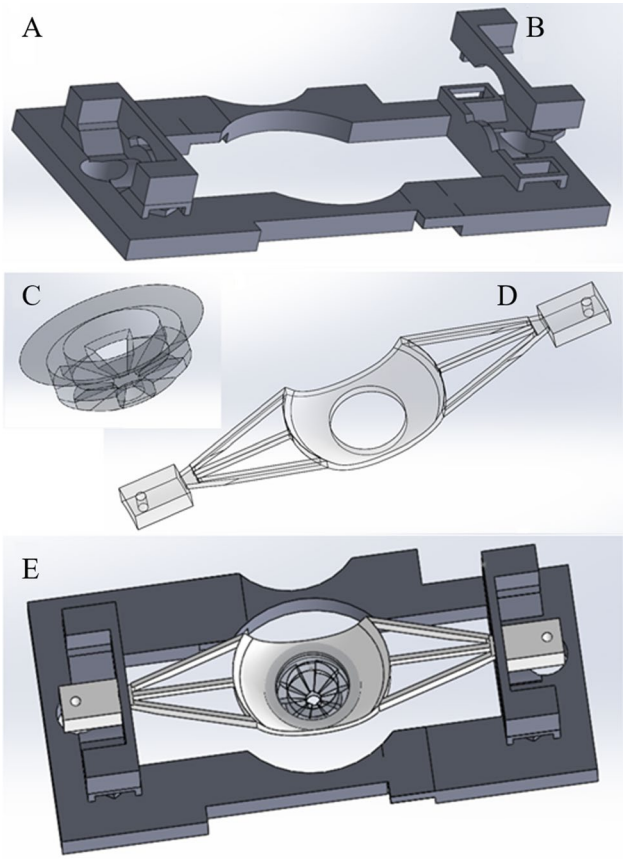

Fig. 1 PICS platform design. **a** Baseplate designed to fit on top of warming system. **b** One of two clips to secure basket to plate. This clip is shown detached. The other clip (left side) is shown in the attached position. **c** Tissue sample cap. **d** Rotation basket with a hole for placement of tissue sample cap. **e** PICS platform fully assembled

Sample stabilizing cap

The LVWM tissue sample is placed in the machined cap for the duration of imaging. This cap is shaped like a steep-sided bowl and stabilizes the sample using the sample's own weight to hold it down into the bowl's center. This allows for imaging without requiring pins or adhesives that may impart shear stress on the tissue or that may deform the sample. Figure 2a shows the cap's interior creates a 5-pronged cavity, with prongs sloped at an angle of 22.6° from the cap's center. This angle is steep enough to ensure the sample falls toward the center, while thin spaces between prongs ensure that the sample itself does not become pinned between the prongs. The top opening of the cap has a diameter of 10.5 mm which allows LVWM samples, dimensions ranging from 7 to 9 mm in length and 5 to 6 mm in width to easily enter the cap. However, the bottom diameter of 3 mm is designed to be smaller than the average size of the LVWMs to prevent the samples from falling through the cap.

Small holes in the cap walls, approximately 2 mm in width, allow artificial cerebrospinal fluid (ACSF) or media to flow throughout the cap and fully immerse the sample. The position of the holes forces fluid to flow up from the bottom of the cap to cover the tissue, preventing shear stresses caused by the flow of ACSF on the imaging face of tissue.

Rotating basket and clip attachments

To rotate the sample beneath the objective, the cap is fitted into a basket. The basket has two extended arms that attach to the baseplate archway via clips (Fig. 2b). Clips are 38.0 mm long and 11.0 mm at their widest point. Clips flex to interlock with the baseplate through grooves on either side of the baseplate arch (most easily visualized in Fig. 1b), and also allow the basket to be easily removed for washing. They form the upper half of the archway, which measures 11.9 mm from end to end and prevent the basket arms from moving off the archway. Clips are tight enough that they allow the basket to remain in place when set at an angle.

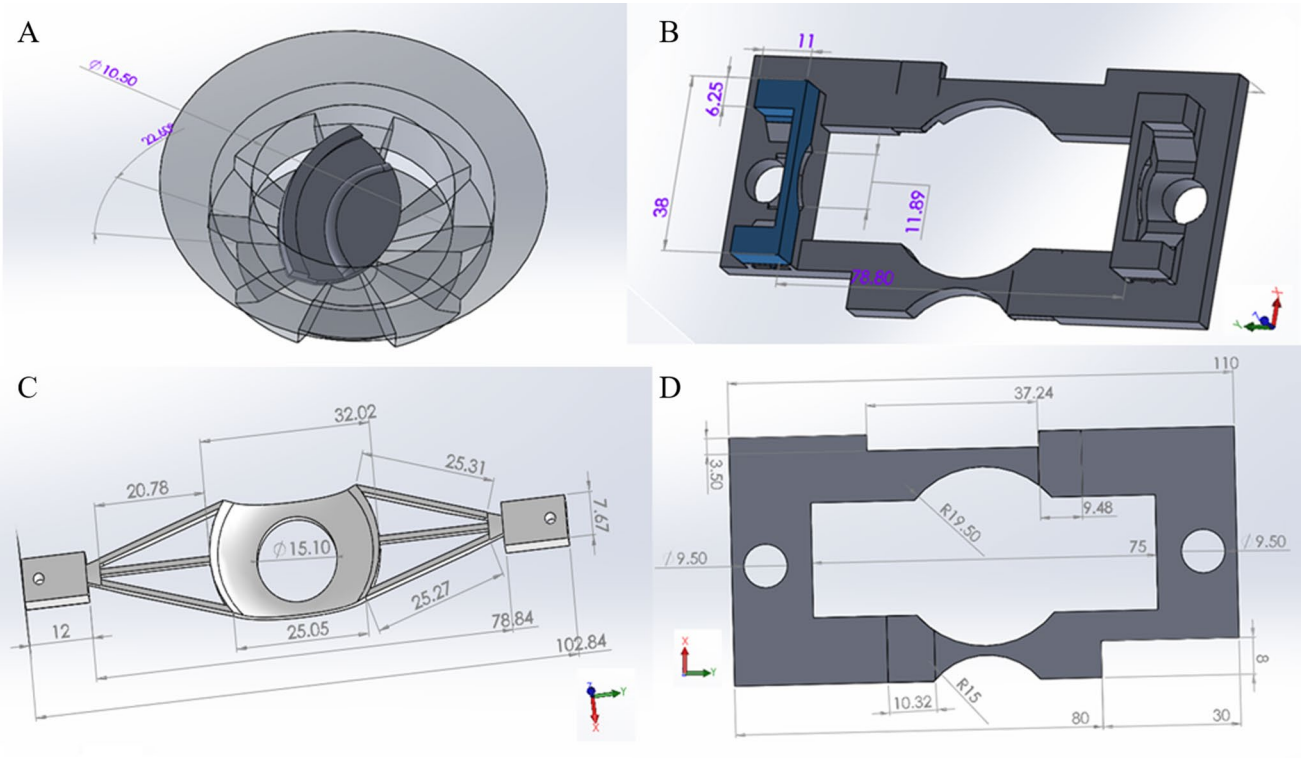

Fig. 2 SolidWorks® PICS dimensions. **a** Sample cap with tissue sample. Diameter 10.5 mm; downward slope of center prongs is 22.6°. **b** Clip dimensions (one clip highlighted in blue). **c** Rotation basket dimensions. **d** Baseplate dimensions; designed to connect securely to temperature controller without interfering with the controller's sensors and fluid handling components

The basket measures 32.0 mm across at its widest point, with a 15.1 mm hole in the center to hold the sample cap (Fig. 2c). Three guide arms are positioned on either end of the basket and meet 34.4 mm from the center, creating a truss-like structure which stabilizes movement of the device by preventing wavering motion on either side. The tapered ends of the arms fit into curved slots which we have termed the axial rotation archway, created by the raised arches on the baseplate and domed arches of the interlocking clips. Blocks measuring 12.0 mm in length complete the opposing ends, providing easier manual manipulation of the device. Open sections were created on both sides of the basket to make the basket usable independent of orientation and to avoid impact with the microscope objective. Care was taken during design to ensure the center of mass and, therefore, center of rotation was near the top of the LVWM tissue sample, designated as the imaging surface. This was accomplished using the SolidWorks® center of mass tool.

Baseplate and the environmental controller interface

A widely used, commercially available controller, the Bioptechs Delta TC3 Culture Dish Micro-Observation Temperature Control System, was chosen to maintain the temperature of samples and to direct fluid flow across the sample. The thin, open base of the PICS system (Fig. 2d) securely connects to the Bioptechs system by encircling two screw posts on each end of the Bioptechs system with 9.5 mm-diameter holes in the PICS base. In the center of the control system is a fluid reservoir that maintains heated media, such as ACSF. The cutout in the center of the baseplate, depicted by the 19.5 mm radius from center, allows the tissue access to the reservoir. The cutout length, 75 mm, is larger than the reservoir both to prevent interference with temperature or fluid controls and to cut down on the amount of printable material used. As the base extends across the entire control system, 110 mm, other cutouts are created to prevent interference with the control system. Due to the versatile nature of 3D printing, a wide range of environmental controllers could be used with minor modifications of the PICS baseplate.

Computer numerical control (CNC) milling

The basket and cap components were manufactured using CNC milling. The models developed in SolidWorks were converted to STL format and imported into Autodesk® Fusion 360™, a 3D cloud-based computer-aided design (CAD)/CAM/computer-aided engineering (CAE) program.

Tool paths were created with accompanying G-code, and then transferred into PathPilot®, control software created by and for Tormach Personal CNCs. A detailed description of the tool paths can be found in Appendix 1.

Animals

Two-to-six-month-old Gad2-eGFP + mice [Tg(Gad2-EGFP) DJ31Gsat/Mmucd; RRID:MMRRC_011849-UCD] were obtained from the Mutant Mouse Regional Resource Center. In LVWM imaging, Gad2 is used as a marker for neuroblasts (Wang et al. 2003). Food and water were provided *ad libitum* and room lighting was on a 12 h on—12 h off cycle. Care of mice and procedures to collect tissue were approved by the Louisiana Tech University Institutional Animal Care and Use Committee. Furthermore, all procedures were in accordance with the National Institute of Health Guide for the Care and Use of Laboratory Animals (NIH Publications No. 80-23, revised 1996).

Tissue extraction

Mice were injected in the lateral tail vein with Texas Red Dextran (Life Technologies Corp.) to allow for visualization of vasculature during imaging. 3 min after injection, mice were sacrificed via cervical dislocation under isoflurane anesthesia, and LVWMs were extracted. Extraction was completed, as previously described (Mirzadeh et al. 2010a). Briefly, using a stereomicroscope, the medial wall was retracted from the lateral ventricle and cut away. The cortex and thalamus were removed to give a clear view of the lateral ventricle.

After dissection of the LVWM was complete, the tissue was immediately placed into the PICS cap, which was then transferred into prewarmed, oxygenated ASCF. The cap and tissue sample were placed into the basket, and then rotated radially to position the desired region for images.

Image acquisition

Images of LVWM tissue were obtained using a Vivo™ 2-Photon Microscopy Workstation [Intelligent Imaging Innovations, Inc. (3i)] with two GaAsP detectors, a fluorescent bandpass filter set for red (612/69 nm) and green (525/40 nm) emission (Semrock, Inc.), a Chameleon Vision II multiphoton laser (Coherent) tuned to 890 nm, and a Pockels cell (Conoptics, Inc.) to attenuate laser power. Slidebook software (3i) was used to control the microscope system and to save and export images as 16-bit TIFF files. Either a Nikon Fluor 40×/0.80 NA water immersion lens or a Nikon 16×/0.80 NA ELWD water immersion lens was employed to obtain images of neuroblasts and surrounding vasculature. In some instances, time-lapse recording was used to capture and track migration (see Appendix 1).

Results

PICS performance

The PICS platform was used to test over 15 samples without requiring repairs or revisions. The machined basket and cap allowed the sample to be adjusted axially and radially during imaging. Samples were stable and able to undergo imaging without excessive refocusing or repositioning. Use of a dipping objective assured that the sample was continually immersed. No decrease in resolution was observed during our imaging sessions. The PICS platform added 1.3 cm in height to the Bioptechs system, resulting in an overall height of 2 cm. The low profile allowed for easy incorporation into the imaging system (Fig. 3a).

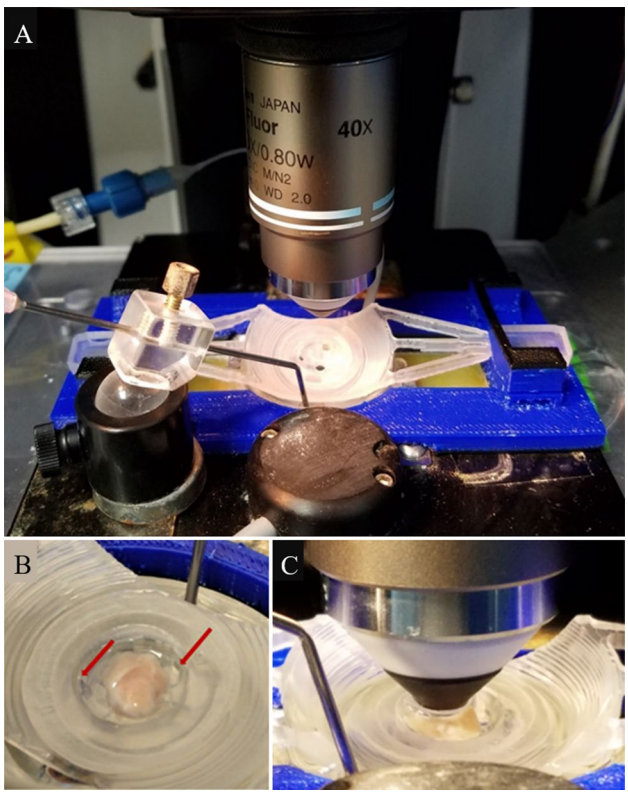

Fig. 3 PICS platform in use. **a** Complete PICS system attached to controller and fluid handling system. Height of PICS platform is 2 cm, including control system. **b** An LVWM rests in the sample cap and remains in place with fluid flowing (arrows show direction of flow). **c** Dipping objective (40×, 2.0 mm WD) is positioned over sample for imaging and full immersion is maintained

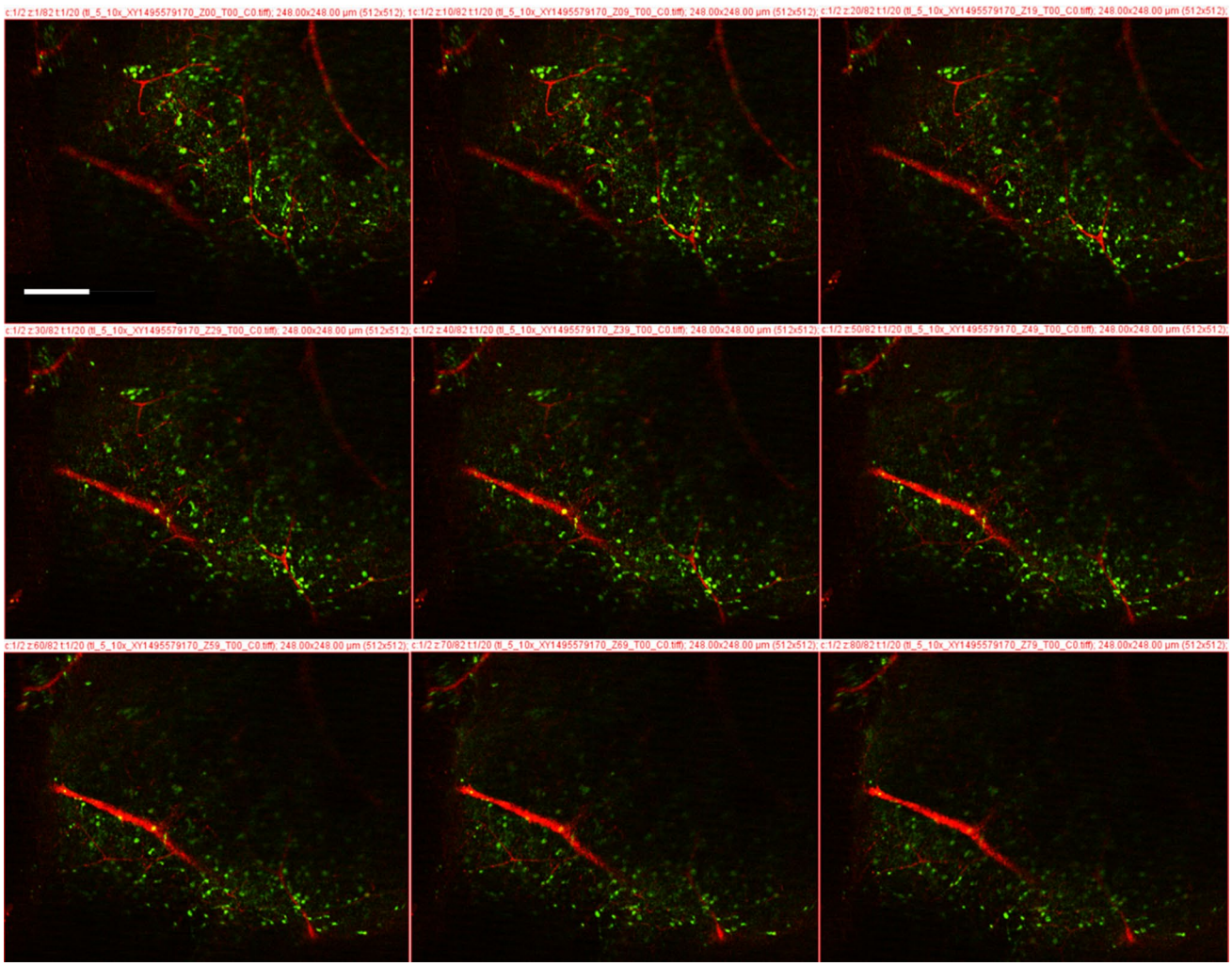

Fig. 4 No lateral movement of sample during imaging. Images are from a Z-stack of an LVWM using a 16×/0.8NA dipping lens and a 1.86 µm step size; volume was 248 × 248 × 150 (µm). These selected image planes are 10 µm apart. GFP was expressed under the Gad2 promoter to visualize neuroblasts (green) in the SVZ. Texas Red Dextran (30 kDa) was injected via the tail vein as a vascular counterstain (red). No lateral translation of the vasculature in the images was observed, suggesting that the sample did not move due to shear forces from fluid flow. Scale bar is 50 µm

Verifying sample stability

Sample stability was evaluated based on the analysis of acquired images. During imaging, the sample was considered stable if tissue lay at rest once placed in the cap, remaining in place when subjected to fluid flow and the movement of the dipping objective. Figure 3b depicts the observed LVWM sample stabilization in the cap with fluid flow, while Fig. 3c depicts full immersion of an LVWM sample for imaging with a dipping objective. During tests, no visible tipping or lateral movement of samples due to fluid flow was observed over 1 h of continual ASCF flow. Furthermore, upon axial or radial rotation, the samples remained in their original position in the sample cap.

Image analysis indicates that there was no unintended lateral movement during capture with the PICS platform. Image planes in Fig. 4 are from a Z-stack acquired while using the device. The image was taken over an 80 µm range in the Z dimension and measures 248 × 248 µm in *X* and *Y*. Had the sample moved during imaging, disruptions in the continuity of features in the Z-stack, such as blood vessels, would appear between planes. All images are in focus and the vasculature, used as landmarks, did not drift in *X* or *Y* as the objective moved in Z.

Verifying sample rotation

Axial archway rotation was tested by sliding the arm along the archway, while the PICS platform was attached to the

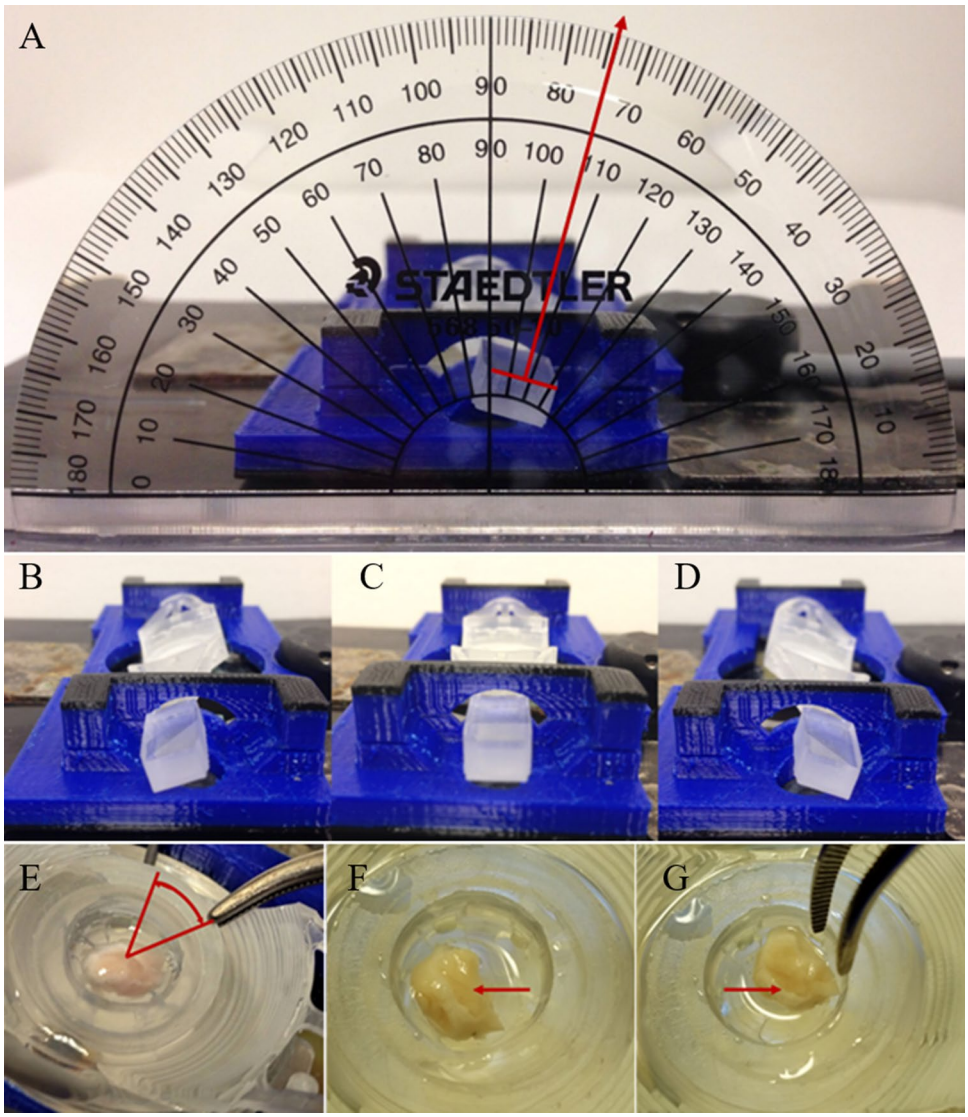

Fig. 5 Positioning basket and sample. **a** Side view of machined device showing ± 16° range of axial rotation. **b–d** Smooth rotation of basket along archway without torsion. **e** Radial rotation of sample cap using forceps. **f, g** Tilting the tissue to allow for other views. Arrows indicate area of focus: inner (**f**) and outer (**g**) curvature

environmental controller. The measured axial rotation of the basket was 16° from center (Fig. 5a) in either direction. The arms moved smoothly along the baseplate arch as shown in Fig. 5b without torsion, while clips prevented motion in other directions. By immobilizing the PICS base, axial rotation of the sample was performed without noticeable translational movement of the sample. Radial rotation of the sample can be achieved using forceps to revolve the sample cap as depicted in Fig. 5c. The sample remains visibly stable inside the cap as the cap itself is turned.

Once the tissue rests in the depression of the sample cap, it remains in that position throughout the full axial rotation of the basket and radial rotation of the cap. However, if views beyond the range of axial and/or radial rotation are necessary, forceps can be used to quickly reposition the sample (Fig. 5d), because it is not glued or pinned. This is a major benefit of using the cap design as there is no risk of damage from removing adhesive or unpinning the sample.

Curved tissue image quality

Multiphoton images of the lateral ventricular wall were taken using the PICS platform to ensure image quality without decrease in SNR throughout imaging. A mosaic comprised of these images was created using Fiji's Stitching plugin (Preibisch et al. 2009) to show the span of a typical LVWM (Fig. 6a). Images were acquired with a 16× dipping objective; 14 images were combined to produce a mosaic view of the cytoarchitecture of the SVZ. The inset, outlined in blue, includes highly detailed images of the LVWM with counterstained vasculature. Images maintain consistent detail throughout the curved tissue.

Higher resolution images, taken with a 40× dipping objective, also show that PICS continues to function

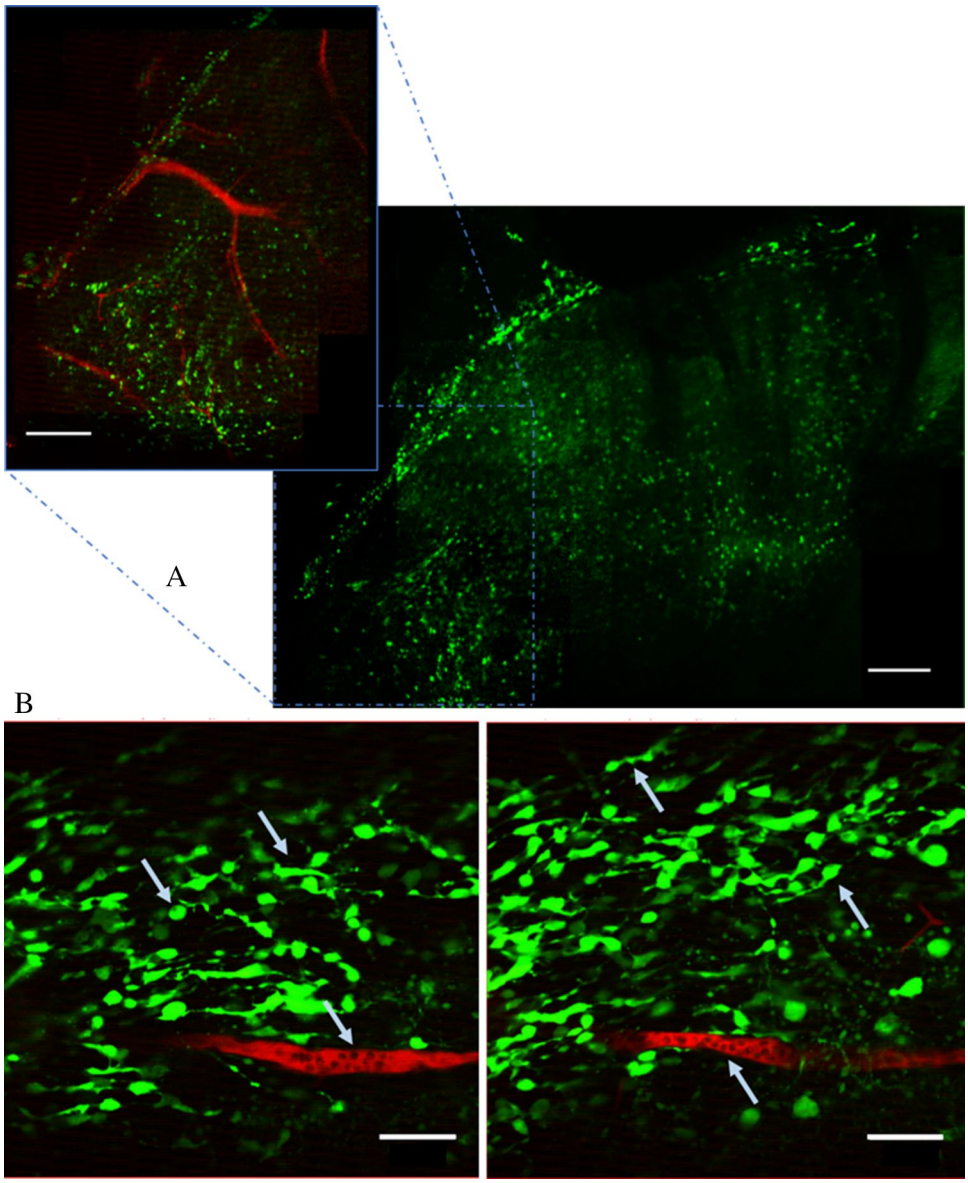

Fig. 6 **a** Mosaic of LVWM using a 16×/0.8 NA dipping lens; 14 tiles complete the curvature of the SVZ. Neuroblasts (green) express GFP under Gad2 promoter. Inset is a more detailed view (blue box) showing counterstained vasculature (red). Scale bar is 50 µm. For stitching, a Fiji plugin (Image J), was used to create mosaics. **b** Higher resolution images of a LVWM using the PICS platform and a 40×/0.8 NA dipping lens. Panels are image planes from a Z-stack 248×248×76 (µm). Arrows denote red blood cells (dark areas in blood vessels), rounded cells, and processes indicating nucleokinesis. Scale bar is 40 µm

as designed when objectives are changed on the microscope. Figure 6 clearly shows branches in the vasculature (Fig. 6a, inset) as well as red blood cells (Fig. 6b). The rounded shape of some neuroblasts are evident, as well as distinctly extended leading or trailing processes, seen in fine detail, that depict the dynamic process of nucleokinesis in migration (Martinez-Molina et al. 2011; Nam et al. 2007).

Discussion

Multiple iterations of the PICS Platform were manufactured before the design was finalized. Early on, the basket and cap components were consolidated, however consolidation eliminated any radial rotation of the sample and added difficulty in creating an appropriately sized bottom opening. Other materials were also tested and subjected to manually applied downward pressure and torque to assess general structural rigidity and expected endurance, including nylon and standard photopolymer resin. These materials were not rigid enough to prevent undesirable torsion on the basket when force was only applied to one of the basket arms. On the other hand, PC was rigid enough to prevent undesirable bending of the basket and arms during axial rotation.

Certain features, such as the cap, basket, and archways, of the base were not amenable to production using standard, single-filament, 3D printing without support material, because they would bend under their own weight before the parts cooled. Removing support material used in the 3D printing process without distorting the design was a key problem. However, these could be produced using a dual extruder that prints a second, dissolvable polymer, such as

high impact polystyrene (HIPS), which fills gaps and prevents deformation before the original polymer cools. After cooling, the dissolvable filament is chemically removed. Utilizing 3D printing for all parts would eliminate the need for milling expertise.

The degree of basket rotation can also be increased without changing the manufacturing methods. As the total arc length traveled along the base arch is inversely related to the thickness of the basket arms, future designs may increase the axial rotation of the basket by reducing the thickness of the attached arms. In addition, the cap design will accommodate a wide size range of tissues without altering its size. However, if the tissue is too large to fit into the cap, then SolidWorks, or a similar design program, can be used to increase the diameter of the top portion of the cap. If the sample is too small to seat securely into the bottom of the cap, then the size of the vanes on the inside of the cap can be enlarged to create a smaller amount of free space to securely hold the tissue. For samples with a different radius of curvature, the arch on Parts A and B (Fig. 1) should be scaled up for tissues with a larger radius of curvature and scaled down for tissue having a smaller radius. Another advantage of the design is that it does not cover the electrode mounting areas on the warmer system; thus, PICS can be used in conjunction with electrophysiology.

In summary, the PICS platform provides an easily incorporated system that reduces the time and difficulty of imaging curved surfaces. Optimized for imaging LVWMs, the device allows researchers to easily maintain a consistent imaging plane on a curved sample without harming the cells within the tissue. Furthermore, its low profile should make it compatible with a wide variety of imaging systems, and the versatility of 3D printing should allow researchers to redesign the base to fit the commercially available environmental controller of their choice.

Acknowledgements We would like to thank Dr. Francis Szele, Oxford University, UK, for inspiring us to create this device and for the use of his Bioptechs TC3 warming system to test the device. Graduate support was provided by a National Institutes of Health grant R21NS090131 (BSK) and a Louisiana Board of Regents Graduate Fellowship (JLS). Funding was also provided by the Edmondson/Crump Endowed Professorship, Louisiana Tech University (TAM).

Compliance with ethical standards

Conflict of interest The authors declare that they have no conflict of interest.

Statement on the welfare of animals All applicable international, national, and/or institutional guidelines for the care and use of animals were followed. All procedures performed in studies involving animals were in accordance with the ethical standards of the Louisiana Tech University Institution Care and Use Committee. This article does not contain any studies with human participants performed by any of the authors.

References

Chang EH, Adorjan I, Mundim MV, Sun B, Dizon ML, V (2016) Traumatic brain injury activation of the adult subventricular zone neurogenic niche. Front Neurosci. https://doi.org/10.3389/fnins.2016.00332

Cheong WF, Prahl SaS, Welch aJA (1990) A review of the optical properties of biological tissues. IEEE J Quantum Electron. https://doi.org/10.1109/3.64354

Comte I, Kim Y, Young CC, Harg JM, Van Der Hockberger P, Bolam PJ, Poirier F, Szele FG (2011) Galectin-3 maintains cell motility from the subventricular zone to the olfactory bulb. J Cell Sci https://doi.org/10.1242/jcs.079954

Cyran CC, Paprottka PM, Eisenblätter M, Clevert DA, Rist C, Nikolaou K, Lauber K, Wenz F, Hausmann D, Reiser MF, Belka C, Niyazi M (2014) Visualization, imaging and new preclinical diagnostics in radiation oncology. Radiat Oncol 9:3. https://doi.org/10.1186/1748-717X-9-3

Darnell DK, Stanislaw S, Kaur S, Antin PB (2010) Whole mount in situ hybridization detection of mRNAs using short LNA containing DNA oligonucleotide probes. RNA 16:632–637. https://doi.org/10.1261/rna.1775610

Fiorelli R, Azim K, Fischer B, Raineteau O (2015) Adding a spatial dimension to postnatal ventricular-subventricular zone neurogenesis Development. https://doi.org/10.1242/dev.119966

Goings GE, Sahni V, Szele FG (2004) Migration patterns of subventricular zone cells in adult mice change after cerebral cortex injury. Brain Res 996:213–226. https://doi.org/10.1016/J.BRAINRES.2003.10.034

Graydon ML, Giorgi PP (1984) Topography of the retinal ganglion cell layer of Xenopus. J Anat 139(Pt 1):145–157

Hagl CI, Wink E, Scherf S, Heumüller-Klug S, Hausott B, Schäfer K-H (2013) FGF2 deficit during development leads to specific neuronal cell loss in the enteric nervous system. Histochem Cell Biol 139:47–57. https://doi.org/10.1007/s00418-012-1023-3

Lennington JB, Yang Z, Conover JC (2003) Neural stem cells the regulation of adult neurogenesis. Reprod Biol Endocrinol 1:99. https://doi.org/10.1186/1477-7827-1-99

Martinez-Molina N, Kim Y, Hockberger P, Szele FG (2011) Rostral migratory stream neuroblasts turn and change directions in stereotypic patterns. Cell Adhes Migr 5:83–95. https://doi.org/10.4161/cam.5.1.13788

Mirzadeh Z, Doetsch F, Sawamoto K, Wichterle H, Alvarez-buylla A (2010a) The subventricular zone en-face: wholemount staining and ependymal flow JoVE. https://doi.org/10.3791/1938

Mirzadeh Z, Han Y-G, Soriano-Navarro M, García-Verdugo JM, Alvarez-Buylla A (2010b) Cilia organize ependymal planar polarity. J Neurosci 30:2600–2610. https://doi.org/10.1523/JNEUROSCI.3744-09.2010

Nagasawa H, Yanai R (1977) Mammary growth and function and pituitary prolactin secretion in female nude mice. Eur J Endocrinol 86:794–802. https://doi.org/10.1530/acta.0.0860794

Nam SC, Kim Y, Dryanovski D, Walker A, Goings G, Woolfrey K, Kang SS, Chu C, Chenn A, Erdelyi F, Szabo G, Hockberger P, Szele FG (2007) Dynamic features of postnatal subventricular zone cell motility: a two-photon time-lapse study. J Comp Neurol 505:190–208. https://doi.org/10.1002/cne

Parra SG, Chia TH, Zinter JP, Levene MJ (2010) Multiphoton microscopy of cleared mouse organs. J Biomed Opt 15:036017. https://doi.org/10.1117/1.3454391

Platel J, Heintz T, Young S, Gordon V (2008) Tonic activation of GLU K5 kainate receptors decreases neuroblast migration in whole-mounts of the subventricular zone J Physiol Banner 16, 3783–3793. https://doi.org/10.1113/jphysiol.2008.155879

Preibisch S, Saalfeld S, Tomancak P (2009) Globally optimal stitching of tiled 3D microscopic image acquisitions. Bioinformatics 25:1463–1465. https://doi.org/10.1093/bioinformatics/btp184

Rosewell IR, Giangreco A (2012) Murine aggregation chimeras and wholemount imaging in airway stem cell biology. Humana Press, Totowa, pp 263–274. https://doi.org/10.1007/978-1-61779-980-8_20

Sasaki H, Hogan BL (1993) Differential expression of multiple fork head related genes during gastrulation and axial pattern formation in the mouse embryo. Development 118:47–59

Shen Q, Wang Y, Kokovay E, Lin G, Chuang S, Goderie SK, Roysam B, Temple S (2008) Article adult SVZ stem cells lie in a vascular niche: a quantitative analysis of niche cell–cell interactions. Cell Stem Cell https://doi.org/10.1016/j.stem.2008.07.026

Strien ME, Van Berge SA, Van Den Hol EM (2011) Migrating neuroblasts in the adult human brain: a stream reduced to a trickle. Nat Publ Gr 21:1523–1525. https://doi.org/10.1038/cr.2011.101

Thévenaz P, Unser M (2007) User-friendly semiautomated assembly of accurate image mosaics in microscopy. Microsc Res Tech 70:135–146. https://doi.org/10.1002/jemt.20393

Udan RS, Piazza VG, Hsu C-W, Hadjantonakis A-K, Dickinson ME (2014) Quantitative imaging of cell dynamics in mouse embryos using light-sheet microscopy. Development 141:4406–4414. https://doi.org/10.1242/dev.111021

Ullmann JFP, Moore BA, Temple SE, Fernández-Juricic E, Collin SP (2012) The retinal wholemount technique: a window to understanding the brain and behaviour. Brain Behav Evol 79:26–44. https://doi.org/10.1159/000332802

Wang DD, Krueger DD, Bordey A (2003) GABA depolarizes neuronal progenitors of the postnatal subventricular zone via GABA A receptor activation J Physiol. https://doi.org/10.1113/jphysiol.2003.042572

Wang C, Liu F, Liu Y, Zhao C, You Y, Wang L, Zhang J, Wei B (2011) Identification and characterization of neuroblasts in the subventricular zone and rostral migratory stream of the adult human brain. Nat Publ Gr 21:1534–1550. https://doi.org/10.1038/cr.2011.83

Young CC, Brooks KJ, Buchan AM, Szele FG (2011) Cellular and molecular determinants of stroke-induced changes in subventricular zone cell migration. Antioxid Redox Signal 14(10):1877–1888. https://doi.org/10.1089/ars.2010.3435

Young CC, Harg JM, Van Der Lewis NJ, Brooks KJ, Buchan AM, Szele FG (2013) Ependymal ciliary dysfunction and reactive astrocytosis in a reorganized subventricular zone after stroke Cereb Cortex. https://doi.org/10.1093/cercor/bhs049

Zhou B, Pu WT (2011) Epicardial epithelial-to-mesenchymal transition in injured heart. J Cell Mol Med 15:2781–2783